Delayed intersubband relaxation in quantum wires due to quantum kinetic Coulomb scattering

F. Prengel and E. Schöll

Institut für Theoretische Physik, Technische Universität Berlin, Hardenbergstraße 36, D-10623 Berlin, Germany

(Received 2 October 1998)

A theoretical analysis of the ultrafast intrasubband and intersubband dynamics of optically excited electrons in quantum wires is presented within the density matrix formalism. It is shown that the inclusion of non-Markovian electron-electron quantum kinetics, in addition to semiclassical optical phonon scattering, is necessary for an appropriate description. In particular, the dynamics of the two-particle density correlations must be explicitly taken into account. The electron-electron scattering processes, which are strongly restricted in quantum wires by energy and momentum conservation, are substantially enhanced on the quantum kinetic level, leading to fast *intrasubband* thermalization, and *intersubband* redistribution of the electrons which substantially delays the phonon-induced intersubband relaxation. Our simulations predict that the influence of electron-electron scattering becomes noticeable already at electron densities per unit length of the order of 10^6 m^{-1}. [S0163-1829(99)09607-1]

I. INTRODUCTION

The availability of femtosecond laser pulses and ultrashort-time spectroscopy[1] in conjunction with, e.g., near-field optical microscopy for nanometer scale resolution[2,3] has brought an increased interest in the nonequilibrium dynamics of electrons in low-dimensional semiconductor nanostructures. They are promising candidates for devices with new features and optimized performance due to their special optical and transport properties, e.g., an increased density of states and strongly modified scattering processes.

Pump-and-probe experiments performed on these structures usually produce excited carriers in their respective bands which relax to the bottom of their bands before they recombine. In low-dimensional structures, this includes intersubband relaxation as well as intrasubband thermalization and subsequent cooling down to the lattice temperature.

Two-dimensional semiconductor systems (quantum wells) have been studied experimentally[4–9] and theoretically[10–14] in detail, while one-dimensional structures (quantum wires) have gained increased attention only recently[15–19] because they might offer even more interesting optoelectronic properties. For example, it is expected that quantum wire lasers exhibit superior performance compared to higher-dimensional laser structures.

In quantum wells the relaxation of electrons from the $n=2$ into the $n=1$ subband leads to significant heating of the electron gas here. The subsequent thermalization is influenced by phonon emission as well as by Coulomb scattering. In a degenerate electron gas, thermalization, i.e., the formation of a heated Fermi distribution, may take as long as 2 ps, which is ascribed to the strong screening of the Coulomb interaction in a Fermi gas.[6] Furthermore, it has been found that the cooling of the electron gas down to the lattice temperature by phonon emission takes approximately 50 ps and is almost independent of the electron density.

Up to now there are only few experiments on intersubband scattering in single quantum wires.[20] Thus, little is known about carrier redistribution after direct optical excitation[21] or carrier capture, i.e., about thermalization and cooling of hot electron distributions in quantum wires. For example, relaxation of hot carriers into the lowest-energy subbands in GaAs fractional-layer superlattice quantum wires has been found to be faster than 0.5 ps and 1.5 ps, respectively, for two sets of quantum wires with different dimensions.[21] The expected phonon bottleneck has not been observed.

Measurements of hot carrier relaxation in arrays of GaAs V-groove quantum wires,[22] however, have found intersubband relaxation times of several hundred picoseconds. This might be explained by (a) the intersubband splitting which was smaller than the longitudinal-optical (LO) phonon energy (due to the relatively large cross section of the wires under investigation), therefore electron-phonon scattering could not effectively contribute to the relaxation process, and (b) the high electron density in the sample (of the order of 10^8 m^{-1}), which led to degeneracy effects and therefore inefficient Coulomb scattering due to Pauli blocking.

Investigations on the capture of electrons in a vicinal-step quantum wire from the surrounding quantum well have been performed using a combination of near-field optical microscopy and time-resolved photoluminescence spectroscopy[18] with a spatial resolution of 200 nm. Effective diffusion lengths (several μm) as well as recombination times (2 ns for the quantum well, 1.5 ns for the wire) have been estimated.

Future experimental investigations with improved femtosecond spectroscopy and higher spatial resolution, together with perfected sample growth, are necessary to give more insight into the nonequilibrium electron dynamics and carrier redistribution in a quantum wire.

It is the purpose of this paper to provide a detailed theoretical study and, in particular, make numerical predictions on the influence of electron-electron scattering upon the intrasubband and intersubband dynamics of nonequilibrium electrons in quantum wires. Quantum kinetic effects are anticipated to be particularly pronounced in quasi-one-dimensional structures due to their confined phase space,

　　　　PRB <u>59</u>　　5806

which results in severe restrictions on semiclassical scattering processes[23] imposed by energy and momentum conservation. Using the density matrix approach[24] we shall derive a closed system of quantum kinetic equations for the electron distribution functions in different conduction subbands, their two-particle density correlations, and the nonequilibrium phonon distribution function, including polar-optical phonon scattering and, in particular, all contributions to the electron-electron interaction. Thereby, memory effects, correlations, and energy-time uncertainty in the electron-electron quantum kinetics are fully taken into account. LO phonon emission and absorption, which is the dominant energy relaxation mechanism, is considered in a semiclassical approximation. Since our focus is on the *conduction subband* dynamics, the generation of a nonequilibrium electron distribution is modeled by a semiclassical optical excitation rate, neglecting the valence band dynamics.

During the last decade, the density matrix formalism in momentum space has been applied to a number of problems in semiconductors, including coherent photogeneration of carriers,[25,26] optics of excitons,[27,28,12] four-wave mixing,[29,9] and electron-phonon scattering in the bulk[30–33] and in heterostructures.[17] Dynamical carrier-carrier interaction, if taken into account, has usually been treated in Hartree-Fock approximation by splitting the two-particle density matrices into products of distribution functions and polarizations, neglecting two-particle correlations. In this way, semiconductor Bloch equations are obtained.[34,35]

The inclusion of the two-particle density correlations as separate dynamic variables has allowed for the coherent quantum mechanical description of impact ionization in bulk semiconductors under the influence of high external electric fields[36] or optical excitation.[37] In a simplified quantum kinetic approach to quantum wires, intersubband impact ionization has been considered,[38] demonstrating the softening of the semiclassical impact ionization threshold on ultrashort-time scales. This approach was subsequently extended to include the full multisubband electron-electron interaction.[39,40] Here we consider the effect of Coulomb quantum kinetics in combination with LO phonon scattering upon intersubband *relaxation* as well as subsequent intrasubband *thermalization* and *cooling*.

II. THEORY

Our approach is based on a multisubband density matrix formalism[24] applied to the conduction subbands of a quantum wire with a rectangular cross section. The Hamiltonian

$$H = H_0 + H_{ee} + H_{ep} \qquad (1)$$

is composed of the quasi-free Hamiltonian H_0 and the electron-electron and electron-phonon interactions H_{ee} and H_{ep}, respectively. The quasi-free Hamiltonian is

$$H_0 = \sum_j \sum_k \epsilon_{j,k} c_{j,k}^\dagger c_{j,k} + \sum_{\mathbf{q}} \hbar \omega_{LO} b_{\mathbf{q}}^\dagger b_{\mathbf{q}}, \qquad (2)$$

where $c_{j,k}^\dagger$ and $c_{j,k}$ are the creation and annihilation operators, respectively, of an electron with wave vector k in the jth subband of the quantum wire, $\epsilon_{j,k}$ is the single-electron energy of an electron with wave vector k in the jth subband,
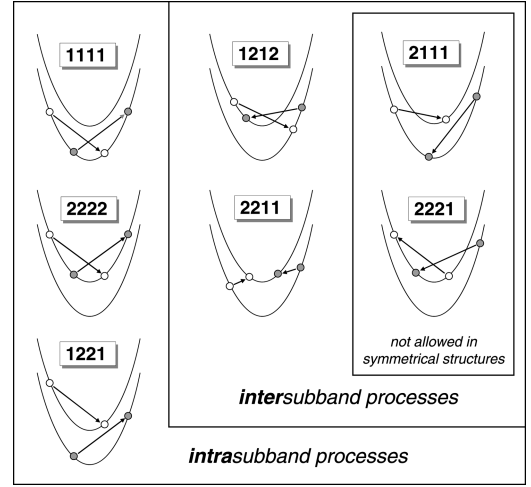

FIG. 1. Electron-electron scattering processes in a two-subband quantum wire. The processes are labeled by indices $i_1' i_2' i_2 i_1$ corresponding to the Coulomb matrix element $V_{i_1' i_2' i_2 i_1}(q)$ where electrons with wave vectors k_1, k_2 in subbands i_1, i_2, respectively, are scattered into states $k_1 + q, k_2 - q$ in subbands i_1', i_2'.

and $b_{\mathbf{q}}^\dagger$ and $b_{\mathbf{q}}$ are creation and annihilation operators, respectively, of a LO phonon with wave vector $\mathbf{q}$ (z component q_z and perpendicular two-dimensional component $\mathbf{q}_\perp$), and $\hbar \omega_{LO}$ is the LO phonon energy.

The Coulomb interaction is given by

$$H_{ee} = \tfrac{1}{2} \sum_{i_1', i_2', i_2, i_1} \sum_{k_1, k_2, q} V_{i_1' i_2' i_2 i_1}(q) c_{i_1', k_1 + q}^\dagger c_{i_2', k_2 - q}^\dagger$$
$$\times c_{i_2, k_2} c_{i_1, k_1}, \qquad (3)$$

where $V_{i_1' i_2' i_2 i_1}(q)$ is the Coulomb matrix element. In the language of second quantization Eq. (3) describes elementary processes where two electrons from subbands i_1 and i_2 with wave vectors k_1 and k_2 are scattered into subbands i_1' and i_2' with wave vectors $k_1 + q$ and $k_2 - q$, respectively (Fig. 1). In the following the shorthand notation $(i_1' i_2' i_2 i_1)$ will be assigned to this process. Note that the following symmetry holds:

$$V_{i_1' i_2' i_2 i_1}(q) = V_{i_1' i_2' i_2 i_1}(-q) = V_{i_2' i_1' i_1 i_2}(q) = V_{i_1 i_2 i_2' i_1'}^*(q). \qquad (4)$$

Therefore, e.g., for a system of two subbands there are only seven different elementary Coulomb processes, which are shown in Fig. 1. For quantum wire structures with inversion symmetry, as considered here, the processes (2111) and (2221) have vanishing matrix elements. Processes (1111), (2222), (1221), and (1212) do not change the number of carriers in the individual subbands. Process (2211) represents intersubband impact ionization[39,40] since it leads to a net change of the subband occupation.

The electron-phonon interaction is

$$H_{ep} = \sum_{jj'} \sum_k \sum_{\mathbf{q}} [\gamma_{j'j}(\mathbf{q}) c_{j',k+q_z}^\dagger b_{\mathbf{q}} c_{j,k}$$
$$+ \gamma_{jj'}^*(\mathbf{q}) c_{j',k}^\dagger b_{\mathbf{q}}^\dagger c_{j,k+q_z}], \tag{5}$$

where $\gamma_{j'j}(\mathbf{q})$ is the screened Fröhlich matrix element of the dominant polar-optical scattering.[41] Since it is known from the analysis of phonon properties in two-dimensional (2D) and 1D systems that the total effect of confined and interface phonons is close to that of 3D (bulk) phonons,[16,42] we will only consider three-dimensional Fröhlich modes here.

Our primary dynamic variable is the one-particle density matrix

$$f_{i'i}(k) \equiv \langle c_{i',k}^\dagger c_{i,k} \rangle. \tag{6}$$

It is diagonal with respect to the wave vector argument k due to the translational symmetry of the quantum wire structure

in the z direction and comprises the *distribution functions* in the different subbands of the conduction band (real-valued intrasubband density matrices, $i'=i$) and the *intersubband polarizations* (complex-valued intersubband density matrices, $i' \neq i$).

The dynamics of these density matrices can be derived from the Heisenberg equation of motion for the single-particle operator

$$i\hbar \frac{d}{dt}(c_{i',k}^\dagger c_{i,k}) = [c_{i',k}^\dagger c_{i,k}, H]. \tag{7}$$

The temporal change of the expectation values is composed of contributions corresponding to the commutator with H_0, H_{ee}, and H_{ep}:

$$i\hbar \frac{d}{dt} f_{i'i}(k) = (\epsilon_{i,k} - \epsilon_{i_1',k}) f_{i'i}(k)$$

$$+ \sum_{j_1', j_2', j_2, j_1} \sum_{k',q} V_{j_1' j_2' j_2 j_1}(q) \{ \delta_{j_2',i} \langle c_{j_1',k'}^\dagger c_{i',k}^\dagger c_{j_2,k+q} c_{j_1,k'-q} \rangle - \delta_{j_1,i'} \langle c_{j_1',k+q}^\dagger c_{j_2',k'-q}^\dagger c_{j_2,k'} c_{i,k} \rangle \}$$

$$+ \sum_j \sum_{q_z} \sum_{\mathbf{q}_\perp} [\gamma_{ij}(q_z,\mathbf{q}_\perp) \langle c_{i',k}^\dagger b_{\mathbf{q}} c_{j,k-q_z} \rangle - \gamma_{ji'}(q_z,\mathbf{q}_\perp) \langle c_{j,k+q_z}^\dagger b_{\mathbf{q}} c_{i,k} \rangle + \gamma_{ji}^*(q_z,\mathbf{q}_\perp) \langle c_{i',k}^\dagger b_{\mathbf{q}}^\dagger c_{j,k+q_z} \rangle$$

$$- \gamma_{i'j}^*(q_z,\mathbf{q}_\perp) \langle c_{j,k-q_z}^\dagger b_{\mathbf{q}}^\dagger c_{i,k} \rangle]. \tag{8}$$

The first part describes merely a phase-coherent rotation of the polarizations ($i' \neq i$) in the complex plane with a frequency corresponding to the intersubband splitting energy at the respective k value.

The Coulomb interaction of the electrons (H_{ee}) leads to a coupling of the single-particle density matrices to two-particle density matrices $\langle c_{j_1',k_1}^\dagger c_{j_2',k_2}^\dagger c_{j_2,k_2-q} c_{j_1,k_1+q} \rangle$ which can be decomposed into a Hartree-Fock factorized term and a correlated remainder, i.e., the two-particle density correlations $s_{j_1' j_2' j_2 j_1}(k_1,k_2,q)$:

$$\langle c_{j_1',k'}^\dagger c_{j_2',k}^\dagger c_{j_2,k+q} c_{j_1,k'-q} \rangle$$

$$= -f_{j_1' j_2}(k+q) f_{j_2' j_1}(k) \delta_{k',k+q} + s_{j_1' j_2' j_2 j_1}(k',k,-q). \tag{9}$$

The Hartree-Fock contribution in Eq. (9) yields a band renormalization by the self-energy

$$\hbar \Omega_{i_1 i_2}(k) \equiv -\sum_{j_1,j_2} \sum_q V_{j_1 i_1 j_2 i_2}(q) f_{j_1 j_2}(k+q) \tag{10}$$

while the two-particle density correlations describe coherent electron-electron scattering processes.

In our approach the *two-particle density correlations* constitute secondary dynamic variables. The following symmetries hold for these quantities:

$$s_{j_1' j_2' j_2 j_1}(k_1,k_2,q) = s_{j_2' j_1' j_1 j_2}(k_2,k_1,-q), \tag{11}$$

$$s_{j_1' j_2' j_2 j_1}(k_1,k_2,q) = s_{j_1 j_2 j_2' j_1'}^*(k_1+q,k_2-q,-q), \tag{12}$$

$$s_{j_1' j_2' j_2 j_1}(k_1,k_2,q) = s_{j_1' j_2' j_2 j_1}(-k_1,-k_2,-q). \tag{13}$$

The last part of Eq. (8) introduces a coupling to the *phonon-assisted density matrix* $\langle c_{i_1,k+q_z}^\dagger b_{\mathbf{q}} c_{i_2,k} \rangle$ which describes the absorption of a phonon of longitudinal wave vector q_z by an electron of wave vector k in subband i_2 which is scattered to wave vector $k+q_z$ in subband i_1. Since momentum is no good electron quantum number in the x and y directions, the perpendicular momentum component $\mathbf{q}_\perp$ of the phonon is not conserved, but ''absorbed'' by the momentum uncertainty of the electron in the confined x and y directions. The reverse process, phonon emission, is described by the complex conjugate $\langle c_{i_2,k}^\dagger b_{\mathbf{q}}^\dagger c_{i_1,k+q_z} \rangle$.

The hierarchy of equations of motion can be continued by setting up Heisenberg equations for the two-particle density correlations $s_{j_1' j_2' j_2 j_1}(k_1,k_2,q)$ analogous to Eq. (7). Due to the electron-electron interaction, they couple to three-particle

density matrices containing six mode operators.[40] In order to close the system of equations for the primary (distribution functions, intersubband polarizations) and secondary (two-particle density correlations) dynamic variables at this level,[38,43–45] we shall factorize the three-particle density matrices into products of one-particle density matrices and two-particle density correlations, neglecting three-particle density correlations and sums over rapidly oscillating two-particle density correlations which describe screening effects and repeated scattering of electrons[46] as well as five-operator electron-phonon cross terms.[47]

In a full quantum kinetic theory the phonon-assisted density matrices should also be treated as independent dynamic quantities. However, recent work[31,48,33] has shown that the main effect of a quantum kinetic treatment of electron-phonon scattering is an initial broadening of the phonon replica in the emission cascade. More important is the energy relaxation rate provided by phonon scattering, which is already appropriately described in the semiclassical approximation. A comparison of the separate influence of quantum kinetic Coulomb and electron-phonon interaction upon the electron distribution shows that the former is much faster and more pronounced for the electron densities considered here,[40] leading to a considerable broadening of the initial optically generated peak after 50 fs already, whereas the first phonon replica appears later. It is therefore justified to treat the phonons semiclassically. The differential equation for the

phonon-assisted density matrices can be formally integrated in the Markov and adiabatic approximation[47] yielding the energy-conserving semiclassical result

$$\langle c^{\dagger}_{i_1,k+q_z} b_{\mathbf{q}} c_{i_2,k}\rangle$$

$$\approx -i\pi\delta(\epsilon_{i_2,k}-\epsilon_{i_1,k+q_z}+\hbar\omega_{\mathrm{LO}})$$

$$\times\left[\sum_j \left[\gamma^*_{ji_2}(q_z,\mathbf{q}_\perp) f_{i_1 j}(k+q_z)(n_{\mathbf{q}}+1)\right.\right.$$

$$-\gamma^*_{i_1 j}(q_z,\mathbf{q}_\perp) f_{ji_2}(k) n_{\mathbf{q}}\Big]$$

$$-\sum_{jj'} \gamma^*_{jj'}(q_z,\mathbf{q}_\perp) f_{i_1 j}(k+q_z) f_{j'i_2}(k)\Bigg], \qquad (14)$$

where $n_{\mathbf{q}}\equiv\langle b^{\dagger}_{\mathbf{q}} b_{\mathbf{q}}\rangle$ is the *phonon distribution function* which will also be treated as a dynamic variable.

Since in symmetrical structures the electron-electron scattering processes (2111) and (2221) are absent, and since there is no coherent optical intersubband excitation, there are no terms driving the intersubband polarization $f_{12}(k)$, and we can neglect it in our simulations.[47]

The final equations of motion can then be written in the following form:

$$\frac{d}{dt}f_{ii}(k)=-\frac{i}{\hbar}\sum_{j'_1,j'_2,j_2,j_1}\sum_{k',q} V_{j'_1 j'_2 j_2 j_1}(q)\{\delta_{j'_1,i}s_{ij'_2 j_2 j_1}(k,k',q)-\delta_{j_1,i}s_{j'_1 j'_2 j_2 i}(k+q,k'-q,-q)\} \qquad (15)$$

$$+\frac{2\pi}{\hbar}\sum_{\mathbf{q}}\sum_{j} |\gamma_{ij}(q_z,\mathbf{q}_\perp)|^2(\{f_{jj}(k+q_z)[1-f_{ii}(k)](n_{\mathbf{q}}+1)-f_{ii}(k)[1-f_{jj}(k+q_z)]n_{\mathbf{q}}\}\delta(\epsilon_{j,k+q_z}-\epsilon_{i,k}-\hbar\omega_{\mathrm{LO}})$$

$$-\{f_{ii}(k)[1-f_{jj}(k-q_z)](n_{\mathbf{q}}+1)-f_{jj}(k-q_z)[1-f_{ii}(k)]n_{\mathbf{q}}\}\delta(\epsilon_{i,k}-\epsilon_{j,k-q_z}-\hbar\omega_{\mathrm{LO}})),$$

$$i\hbar\frac{d}{dt}s_{i'_1 i'_2 i_2 i_1}(k_1,k_2,q)=\sum_{j_1,j_2}\{\mathcal{E}_{i_1 j_1}(k_1+q)\delta_{i_2,j_2}+\mathcal{E}_{i_2 j_2}(k_2-q)\delta_{i_1,j_1}\}s_{i'_1 i'_2 j_2 j_1}(k_1,k_2,q)$$

$$-\sum_{j'_1,j'_2}\{\mathcal{E}_{j'_1 i'_1}(k_1)\delta_{j'_2,i'_2}+\mathcal{E}_{j'_2 i'_2}(k_2)\delta_{j'_1,i'_1}\}s_{j'_1 j'_2 i_2 i_1}(k_1,k_2,q)$$

$$+\sum_{j'_1,j'_2,j_2,j_1}\bar{V}_{j'_1 j'_2 j_2 j_1}(k_1,k_2,q)\mathcal{F}^{j'_1 j'_2 j_2 j_1}_{i'_1 i'_2 i_2 i_1}(k_1,k_2,q), \qquad (16)$$

where spin degeneracy has been taken into account by defining an *effective Coulomb matrix element*

$$\bar{V}_{j'_1 j'_2 j_2 j_1}(k_1,k_2,q)\equiv 2V_{j'_1 j'_2 j_2 j_1}(q)-V_{j'_1 j'_2 j_1 j_2}(k_1+q-k_2) \qquad (17)$$

(the Coulomb interaction does not lead to spin flips, so both electrons in the exchange term must have the same spin) and an *effective ''phase space filling factor''*

$$\mathcal{F}^{j'_1 j'_2 j_2 j_1}_{i'_1 i'_2 i_2 i_1}(k_1,k_2,q)$$

$$\equiv f_{i'_1 j_1}(k_1) f_{i'_2 j_2}(k_2)[\delta_{j'_1,i_1}-f_{j'_1 i_1}(k_1+q)]$$

$$\times[\delta_{j'_2,i_2}-f_{j'_2 i_2}(k_2-q)]-f_{j'_1 i_1}(k_1+q) f_{j'_2 i_2}(k_2-q)$$

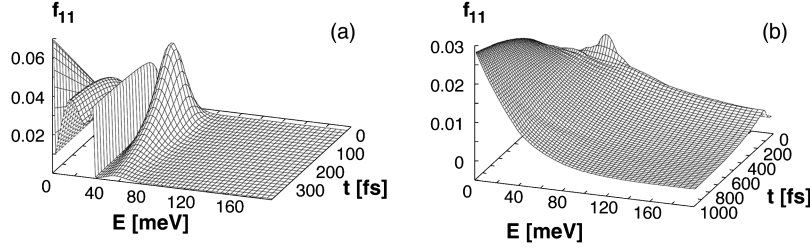$$\times[\delta_{i'_1,j_1}-f_{i'_1 j_1}(k_1)][\delta_{i'_2,j_2}-f_{i'_2 j_2}(k_2)] \qquad (18)$$

FIG. 2. Evolution of a nonequilibrium electron distribution (generated by a Gaussian pulse with $g_0 = 10^{12}$ s^{-1} and $\delta E = 15$ meV at $\bar{E} = 50$ meV) in a semiclassical phonon bath ($T_L = 10$ K) (a) without and (b) with quantum kinetic Coulomb scattering. The total generated electron density is $n = 3.785 \times 10^6$ m^{-1} corresponding to a volume density $n^{3D} = n/(ab) = 5.05 \times 10^{16}$ cm^{-3}. (See Table I for numerical parameters.)

and *renormalized single-particle energies*

$$\mathcal{E}_{ij}(k) \equiv \epsilon_{i,k}\delta_{i,j} + \hbar\Omega_{ij}(k) \tag{19}$$

have been defined.

From Eqs. (15) and (16) it can be seen that electron-electron scattering is described as a coherent two-step process: first the Coulomb interaction builds up two-particle correlations between the carriers; in a second step, scattering between the correlated states takes place. Since the two-particle correlations are independent dynamic variables, the quantum dynamics—with respect to the one-particle densities alone—is non-Markovian. Electron-phonon scattering is described by semiclassical emission and absorption rates.

Similarly, one obtains for the nonequilibrium phonon distribution

$$\frac{d}{dt}n_{\mathbf{q}} = \frac{2\pi}{\hbar}\sum_k\sum_{i,j}|\gamma_{ij}(q_z,\mathbf{q}_\perp)|^2$$

$$\times\{f_{ii}(k+q_z)[1-f_{jj}(k)](n_{\mathbf{q}}+1)$$

$$-f_{jj}(k)[1-f_{ii}(k+q_z)]n_{\mathbf{q}}\}$$

$$\times\delta(\epsilon_{i,k+q_z}-\epsilon_{j,k}-\hbar\omega_{LO}). \tag{20}$$

The terms with $i=j$ describe emission (terms with $n_{\mathbf{q}}+1$) and absorption (terms with $n_{\mathbf{q}}$) of phonons by intrasubband scattering, while the terms with $i\neq j$ account for intersubband phonon scattering.

III. INTRASUBBAND THERMALIZATION

The density matrix formalism will now be applied to investigate the relaxation of a highly excited electron population generated in the upper subband by an optical pulse. In order to conceptually separate the effects of intersubband relaxation and intrasubband thermalization and cooling, we will first discuss a single one-dimensional subband in a quantum wire where a nonequilibrium electron distribution is generated by a semiclassical Gaussian generation rate included in the right-hand side of Eq. (15),

$$g_{opt}(k,t) \equiv g_0 e^{-[(\epsilon_{1,k}-\bar{E})/\delta E]^2}e^{-[(t-\bar{t})/\tau]^2}, \tag{21}$$

which models a Fourier-limited optical pulse of $\delta E = 15$ meV width and $\tau = 44$ fs duration (corresponding to

full widths at half maximum of 25 meV and 73 fs, respectively) centered at $\bar{E} = 50$ meV and $\bar{t} = 50$ fs. As initial conditions we assume $f_{ij}(k) = 0$ $\forall k$ and $s_{ijkl}(k_1,k_2,q) = 0$ $\forall k_1,k_2,q$ for the electrons, and an equilibrium Bose distribution at temperature T_L for the phonons.

The Coulomb matrix elements and the Fröhlich coupling constants are calculated for a quantum wire with rectangular cross section of 5nm×15nm and infinitely high confining potential, and parabolic one-dimensional subbands.

Under the influence of polar-optical phonon scattering alone, the usual formation of phonon replicas can be observed [Fig. 2(a)] at multiples of $\hbar\omega_{LO} = 36$ meV below $\bar{E}$ (see Table I for numerical parameters). The phonon emission threshold of 36 meV where the phonon scattering rate is divergent leads to the discontinuity in the distribution function superimposed on the replica. Electrons with an energy below 36 meV cannot emit optical phonons, therefore no approach of an equilibrium (i.e., Boltzmann) distribution determined by the lattice temperature T_L and the Fermi energy E_F can be expected. Furthermore, even a quantum kinetic treatment of electron-phonon scattering cannot provide this equilibration, as previous work has shown.[49,48,50,51] Note that acoustical phonon scattering would drive the system towards equilibrium on a much slower time scale only.

This situation is not changed by *semiclassical* electron-electron interaction, since intrasubband Coulomb scattering vanishes in quantum wires due to the required conservation of momentum *and* energy in each scattering event.

In a quantum kinetic approach, however, energy conservation may be violated on ultrashort-time scales, which enables electron redistribution by intrasubband Coulomb scattering. The inclusion of quantum kinetic electron-electron interaction thus leads to a totally different evolution of the

TABLE I. Numerical parameters for GaAs used in the simulations.

Parameter	Symbol	Value
x width of quantum wire	a	15 nm
y width of quantum wire	b	5 nm
Conduction subband splitting	$\Delta E = E_2 - E_1$	75 meV
LO phonon energy	$\hbar\omega_{LO}$	36 meV
Effective dielectric permittivity	$\varepsilon_p = \varepsilon_0\varepsilon$	5.639×10^{-10} F m^{-1}
Effective electron mass	m^*	$0.067m_e$

distribution function. The result of a simulation including both electron-phonon and electron-electron interaction is presented in Fig. 2(b) for a lattice temperature of $T_L = 10$ K. Comparison with the case without Coulomb scattering [Fig. 2(a)] reveals the profound qualitative difference: the phonon emission threshold at 36 meV and the phonon replicas are completely absent at later times. Instead, a broad distribution is observed which has its maximum at the bottom of the subband, at $k = 0$, and seems to become steeper with time, eventually approaching a Boltzmann-like, exponentially decreasing function. The equilibrium Boltzmann distribution function, however, is considerably sharper at $T_L = 10$ K. Thus, we obtain a hot electron distribution, and the electrons still must lose energy in a cooling process which finally yields an electron temperature that is equal to the temperature of the crystal lattice.

When the lattice temperature is increased, a higher background density of equilibrium phonons is present. At $T_L = 77$ K no significant difference to the low-temperature case of Fig. 2(a) is visible. At room temperature ($T_L = 300$ K) a new feature emerges: a phonon replica *above* the initial maximum, at $E = 86$ meV. It is a result of the absorption of phonons from the equilibrium heat bath. The phonon density n_q in this case is large enough for phonon absorption processes to give a visible contribution to the electron dynamics.

Figure 3(a) shows the evolution of the nonequilibrium electron distribution for $T_L = 300$ K. The initial Gaussian-shaped nonequilibrium electron distribution (solid line) becomes broad and tends towards the slope of a Boltzmann distribution (thick gray line) after 2 ps already though there are still distinct deviations. In this case, the large equilibrium phonon background (i.e., the ''warm'' phonon bath) seems to provide effective cooling.

To investigate the cooling process in more detail, we introduce an *effective electron temperature* T_e by the second moment of the nonequilibrium distribution function

$$\frac{\hbar^2}{2m^*}\langle k^2 \rangle = \frac{1}{2}k_B T_e. \tag{22}$$

The time dependence of this electron temperature is displayed in Fig. 3(b). A clear tendency from the initial high temperature (''hot'' electrons) to the lower lattice temperature (thin solid lines) is observed in both cases. While the temperature is monotonically decreasing in the semiclassical (sc) case (without Coulomb interaction), there is an initial temperature increase peaking at about 100 fs in the simulations which include quantum kinetic (qk) electron-electron scattering. It must be ascribed to the buildup of two-particle correlations which leads to an increase in the mean kinetic energy per electron since the sum of the (negative) correlation energy and the (positive) kinetic energy decreases only on a slower time scale due to phonon scattering. This is an interesting many-body effect inherent in the quantum kinetics at very early times.

We note further that at $T_L = 300$ K, $T_e \approx T_L$ is reached after 2 ps already in the quantum kinetic case, whereas the electron temperature remains above the lattice temperature even at later times in the case without Coulomb scattering. The reason for this is that electrons with energies E
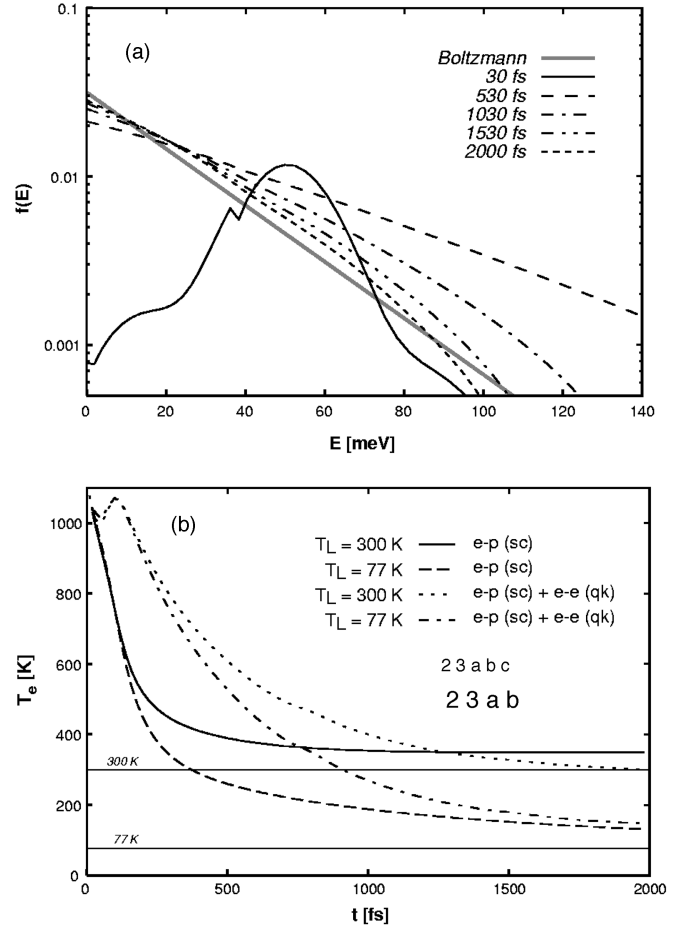

FIG. 3. (a) Evolution of a nonequilibrium electron distribution generated by a Gaussian pulse with $g_0 = 10^{12}$ s^{-1} for a lattice temperature of $T_L = 300$ K with quantum kinetic Coulomb scattering (semilogarithmic plot versus energy). The total generated electron density is $n = 3.785 \times 10^6$ m^{-1} corresponding to a volume density $n^{3D} = n/(ab) = 5.05 \times 10^{16}$ cm^{-3}. The thick gray line represents the equilibrium Boltzmann distribution. (b) Time dependence of the electron temperature T_e in the simulations without [e-p (sc)] and with quantum kinetic Coulomb scattering [e-p (sc) + e-e (qk)] for two different lattice temperatures T_L. (See Table I for numerical parameters.)

$\leqslant 36$ meV are not subject to further scattering processes in which they could transfer part of their energy to the lattice. Some excess energy will therefore remain in the electron gas, keeping it ''hotter'' than the crystal lattice.

Other interesting information which is delivered by our full dynamic simulations concerns the distribution of nonequilibrium phonons. Due to the emission of phonons by the relaxing electrons, additional phonon peaks on the equilibrium background are observed in the semiclassical simulation.[47] The height of these peaks decreases with increasing wave vector since the Fröhlich matrix element which determines the strength of the emission processes is a decreasing function of the phonon wave vector. In the full quantum kinetic simulation a broad phonon distribution is observed because no distinct maxima of the electron distribution are left after as little as 100 fs.

In Fig. 4 we show the time dependence of the different contributions to the total electron energy $\langle H_0^e + H_{ee} \rangle$ for $T_L = 77$ K:
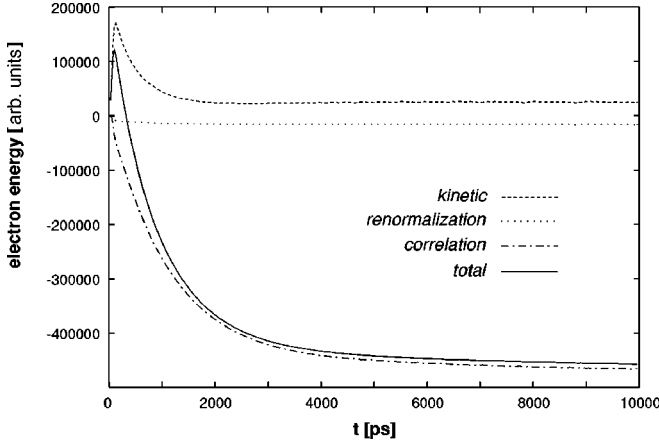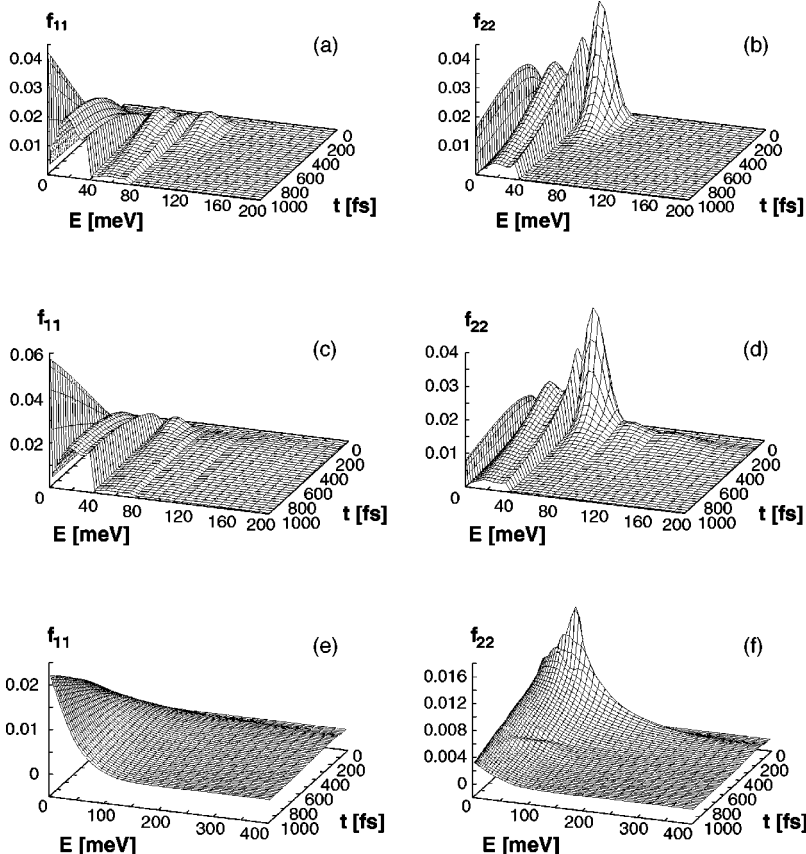
FIG. 4. Different contributions to the total electron energy for the quantum kinetic simulation shown in Fig. 3(b) (for $T_L = 77$ K).

$$E_{\text{kin}} = \sum_j \sum_k \epsilon_{j,k} f_{jj}(k) \qquad \text{(kinetic energy)}, \qquad (23)$$

$$E_{\text{ren}} = -\frac{1}{2} \sum_{i_1' i_2' i_2 i_1} \sum_{k_1} f_{i_1' i_2}(k_1) \sum_q V_{i_1' i_2' i_2 i_1}(q) f_{i_2' i_1}(k_1 + q)$$

(renormalization energy, due to Hartree-Fock part of H_{ee}), (24)

$$E_{\text{cor}} = \frac{1}{2} \sum_{i_1' i_2' i_2 i_1} \sum_{k_1 k_2 q} V_{i_1' i_2' i_2 i_1}(q) s_{i_1' i_2' i_2 i_1}(k_1, k_2, q)$$

(correlation energy). (25)

The correlation energy, which reflects the interaction between the electrons, is gradually built up and tends asymptotically to a large negative constant value. The strongly correlated electron gas then behaves effectively like a gas of *noninteracting* quasiparticles in contact with a heat bath (the background equilibrium phonons).

IV. INTERSUBBAND RELAXATION

If electrons are generated in the second subband of a two-subband system, they will relax to the first subband by phonon emission and Coulomb scattering, as well as redistribute within the subbands. A numerical example of the resulting dynamics is given in Fig. 5, which shows the evolution of the electron distribution functions in the upper and lower subband after optical generation of a nonequilibrium electron population in the upper subband according to Eq. (21) for three different model approximation.

In Figs. 5(a) and 5(b) semiclassical electron-phonon scattering only is taken into account. As expected, we observe phonon replicas in the upper and lower subbands. The formation of an equilibrium electron distribution *within* the subbands, however, cannot be observed.

This situation essentially is not changed by incorporating semiclassical Coulomb interaction into the simulation [Figs. 5(c) and 5(d)]. We recognize additional peak structures above the main peak in the upper subband due to the Coulomb scattering processes (1221) and (1122). The electron redistribution between the subbands, i.e., the relaxation down to the first subband, is slightly faster in this case since there is an additional scattering process, i.e., intersubband Coulomb scattering. The electron distribution functions, how-

FIG. 5. Temporal evolution of the electron distribution function in the lower (f_{11}) and upper (f_{22}) subband, where electrons are generated by a Gaussian pulse with $g_0 = 10^{12}$ s^{-1} (corresponding to $n = 3.785 \times 10^6$ m^{-1}) in the upper subband. The lattice temperature is $T_L = 10$ K. (a), (b) Semiclassical electron-phonon scattering only; (c), (d) semiclassical electron-phonon *and* semiclassical Coulomb scattering; (e), (f) semiclassical electron-phonon and quantum kinetic Coulomb scattering.
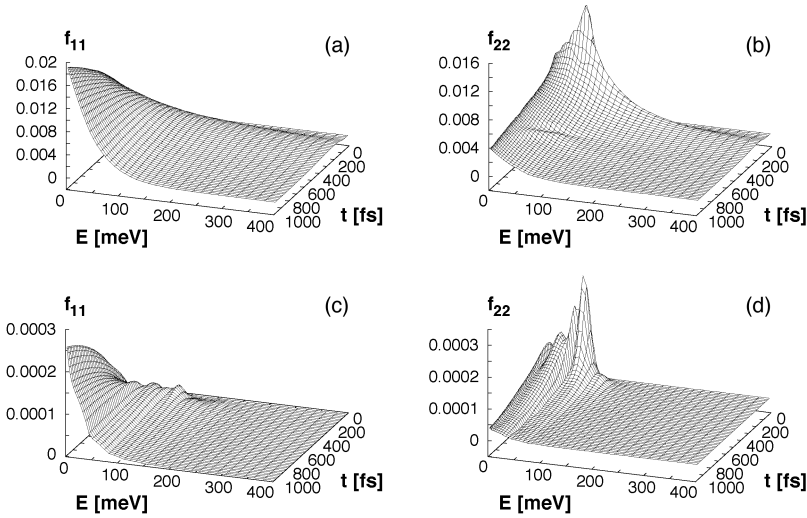
FIG. 6. Temporal evolution of the electron distribution function in the lower (f_{11}) and upper (f_{22}) subband at room temperature ($T_L = 300$ K) for (a), (b) high ($g_0 = 10^{12}$ s^{-1} corresponding to $n = 3.785 \times 10^6$ m^{-1}) and (c), (d) low ($g_0 = 10^{10}$ s^{-1} corresponding to $n = 3.785 \times 10^4$ m^{-1}) laser intensity with semiclassical electron-phonon scattering and quantum kinetic Coulomb scattering. Other parameters as in Fig. 5.

ever, do not approach a Boltzmann distribution. This is due to the absence of any semiclassical intrasubband scattering, therefore the evolution of f_{11} and f_{22} in their respective subbands is comparable to the one already known from Figs. 5(a) and 5(b). No proper thermalization can be achieved in this approach. The purely semiclassical model thus turns out to yield no adequate description of intersubband relaxation.

As Figs. 5(e) and 5(f) demonstrate, only the combined model of quantum kinetic Coulomb interaction (including two-particle correlations) plus semiclassical electron-phonon scattering seems to provide reasonable results. Boltzmann-like distribution functions are formed in both subbands, and these with increasing time approach thermal equilibrium with the surrounding crystal lattice, i.e., $T_e = T_L$.

Figure 6 illustrates the dependence upon lattice temperature and electron density. It shows simulations for room temperature and a higher [Figs. 6(a) and 6(b)] and a lower [Figs. 6(c) and 6(d)] electron density. The time dependence of f_{11} and f_{22} in Figs. 6(a) and 6(b) is very similar to that shown in Figs. 5(e) and 5(f). The only noticeable difference is the steeper f_{11} distribution in Figs. 5(e) and 5(f), compared to Fig. 6(a). This difference can be expected to become more prominent at later times since it takes rather long for a distribution to cool down to lower temperatures, whereas thermal equilibrium at $T_L = 300$ K is established after as little as a few picoseconds.

At lower electron densities [Figs. 6(c) and 6(d)] there remains some fine structure after a longer time which is reminiscent of the early phonon replicas. The intrasubband Coulomb scattering is simply too weak to smooth out these structures sufficiently fast. It is expected that they are eventually removed, possibly only after some nanoseconds. Figures 6(c) and 6(d) reveal that nevertheless the distribution functions f_{11} and f_{22} are close to an equilibrium Boltzmann distribution already after 1 ps. In the higher-density case [Figs. 6(a) and 6(b)] this approach seems to take longer. This can be explained by stronger intersubband impact ionization (2211) which transfers a considerable amount of electrons back into the upper subband, thus slowing down the relaxation process. This phenomenon will now be investigated in detail.

An intersubband relaxation time τ_r can be introduced by assuming that the depletion of the higher subband is approximately exponential:

$$n_2(t) \sim e^{-t/\tau_r}. \tag{26}$$

For semiclassical electron-phonon scattering alone [Fig. 7(a)] the relaxation times are estimated from our simulations as $\tau_r = 0.61$ ps for $T_L = 10$ K and $\tau_r = 0.56$ ps for $T_L = 300$ K. The slightly lower value in the latter case is probably a result of additional *stimulated* phonon emission which is practically absent in the low-temperature phonon bath.

In the simulations with semiclassical electron-phonon and quantum kinetic Coulomb scattering [Fig. 7(b)] a very different behavior is found. Initially, relaxation is faster than with electron-phonon scattering alone, but for larger times (between 300 and 400 ps) there is a crossover behavior, and relaxation becomes much slower with increasing temperature. The relaxation times are estimated as $\tau_r = 0.52$ ps for $T_L = 10$ K and $\tau_r = 0.74$ ps for $T_L = 300$ K. This behavior cannot be explained by semiclassical electron-electron scattering, which does not reproduce the strong temperature dependence and yields only a slight change compared to electron-phonon scattering alone at $T_L = 300$ K ($\tau_r = 0.57$ ps), while the relaxation is faster at $T_L = 10$ K ($\tau_r = 0.50$ ps). Furthermore, in the quantum kinetic simulations, the intersubband relaxation time exhibits a strong dependence upon the exciting laser intensity at 300 K [Fig. 7(c)]. The quantum kinetic electron-electron scattering leads to shorter relaxation times below 0.5 ps for low electron densities up to $n \approx 4 \times 10^5$ m^{-1} (corresponding to $n^{3D} \approx 5.3 \times 10^{15}$ cm^{-3} or $g_0 = 10^{11}$ s^{-1}). At higher electron densities, relaxation is slowed down considerably. This is due to the increased strength of Coulomb interaction at higher densities, which causes stronger intersubband impact ionization [process (2211) in Fig. 1]. By the latter process, electrons which have relaxed down to the first subband by phonon emission are scattered back into the second subband, which effectively diminishes the relaxation rate.

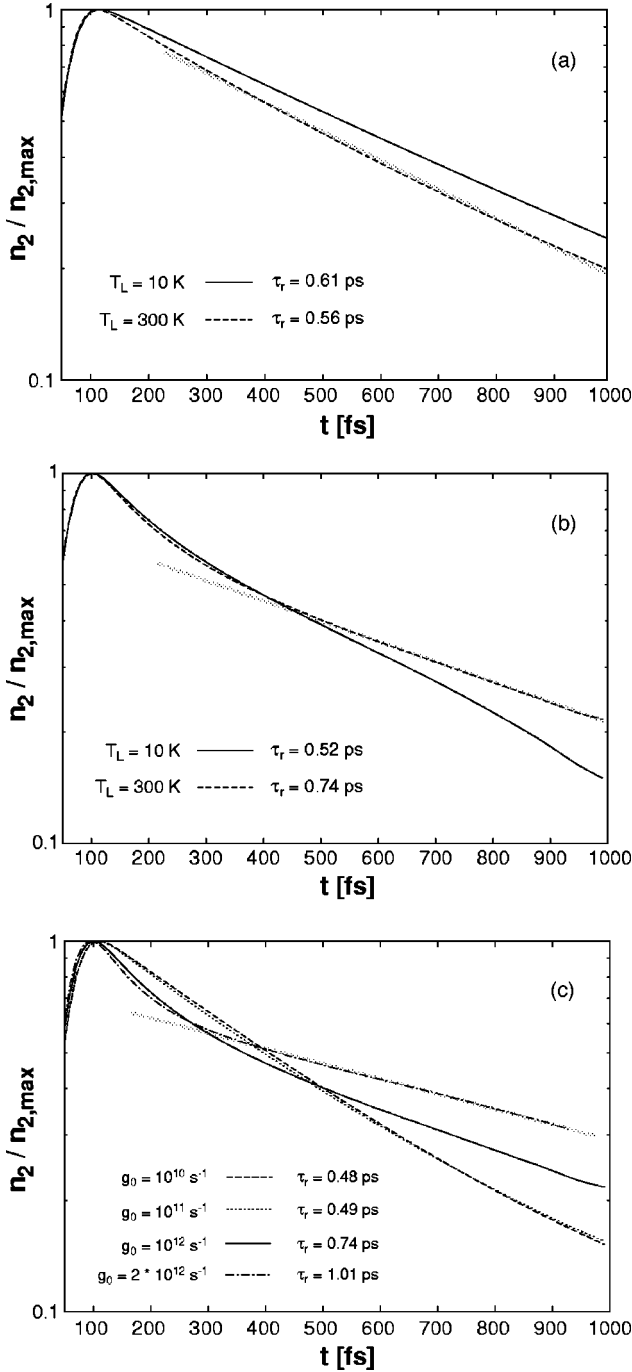To gain more physical insight, we have calculated the ratio

FIG. 7. Semilogarithmic plot of the relative occupation $n_2/n_{2,\text{max}}$ of the upper subband versus time (a) for electron-phonon scattering only, with $g_0=10^{12}$ s^{-1} [black solid line: $T_L=10$ K, as in Figs. 5(a) and 5(b); black dashed line: $T_L=300$ K]. The gray line demonstrates the relaxation time approximation for 300 K according to Eq. (26). (b) For the full quantum kinetic simulations, with $g_0=10^{12}$ s^{-1} [black solid line: $T_L=10$ K, as in Figs. 5(e) and 5(f); black dashed line: $T_L=300$ K, as in Figs. 6(a) and 6(b)]. (c) For the full simulations shown in Fig. 6 for different excitation intensities at $T_L=300$ K. The solid gray line shows a fitted exponential decay corresponding to a relaxation time $\tau_r=1.01$ ps.

$$r_{e\text{-}p}=\frac{\dot{n}_2^{ee}}{\dot{n}_2^{ep}} \qquad (27)$$
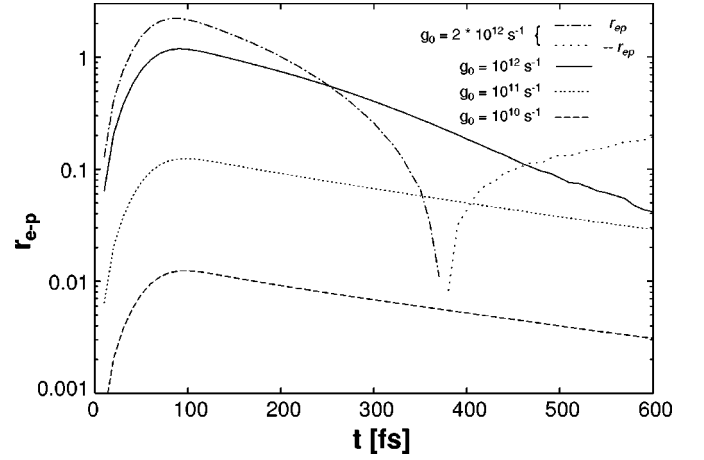
of the electron-electron relaxation rate

FIG. 8. Semilogarithmic plot of the ratio $|r_{e\text{-}p}|$ of electron and phonon scattering rates versus time for the full simulations shown in Fig. 7(c). For $g_0=2\times10^{12}$ s^{-1}, the sparsely dotted line corresponds to $r_{e\text{-}p}<0$.

$$\dot{n}_2^{ee}=(2/L)\sum_k \frac{d}{dt}f_{22}(k)\Big|_{ee} \qquad (28)$$

and the electron-phonon relaxation rate

$$\dot{n}_2^{ep}=(2/L)\sum_k \frac{d}{dt}f_{22}(k)\Big|_{ep}, \qquad (29)$$

which characterizes the relative strength of both scattering mechanisms. Since the electron-electron relaxation rate is roughly proportional to n_2^2, whereas the electron-phonon relaxation rate depends linearly upon n_2, the ratio is expected to decrease in time proportionally to n_2. Figure 8 reveals that Coulomb scattering is much weaker than electron-phonon scattering at low electron densities. Furthermore, its relative strength decreases exponentially with time, due to the depopulation of the upper subband. There is only a very slight increase of the relaxation time with electron density, due to electron-electron scattering.

At $g_0=10^{12}$ s^{-1} (corresponding to $n=3.785\times10^6$ cm^{-1}), both interactions are of comparable strength initially, and the ratio decreases *faster* than exponentially. This explains that initially relaxation is faster than with phonon scattering only, due to the additional scattering channels, but after several hundred picoseconds the relaxation rate slows down, as the electrons are redistributed, leading to a noticeable increase of the corresponding relaxation time in Fig. 7(c). For even higher excitation intensity ($g_0=2\times10^{12}$ s^{-1}), the ratio $r_{e\text{-}p}$ even changes sign. This means that at this point intersubband impact ionization (2211) becomes stronger than Coulomb-induced intersubband relaxation. There is then a net transfer of electrons from the second to the first subband due to electron-phonon scattering, which is diminished by a net transfer in the opposite direction due to Coulomb scattering. This delays the effective relaxation process considerably.

V. CONCLUSIONS

Our theoretical and numerical analysis has shown that the ultrafast intrasubband and intersubband dynamics of non-

equilibrium electrons in quantum wires can be appropriately described only by including electron-electron quantum kinetics, in addition to semiclassical polar-optical phonon scattering. The dynamics is non-Markovian with respect to the electron distribution function and exhibits features of a strongly correlated (though nondegenerate) one-dimensional electron gas. In particular, the dynamics of the electron-electron correlations is explicitly taken into account. The intrasubband and intersubband electron-electron scattering processes, which are strongly restricted in quantum wires by energy and momentum conservation in a semiclassical framework, are substantially enhanced on the quantum kinetic level. This leads to fast *intrasubband* thermalization, and *intersubband* redistribution of the electrons which substantially delays the phonon-induced intersubband relaxation after a short initial phase of accelerated relaxation. From our simulations, we have obtained intersubband relaxation times in the (sub)picosecond range for different lattice temperatures and electron densities. The influence of electron-electron scattering becomes noticeable already at electron densities per unit length of the order of 10^6 m^{-1} corresponding to volume densities of 10^{16} cm^{-3}. The increase of the intersubband relaxation time τ_r at higher densities is due to increased intersubband impact ionization, which transfers electrons from the first subband back to the second, thus inhibiting the relaxation process. While the electron-phonon scattering rate depends linearly on the electron density n, the impact ionization rate depends on the square of n and therefore has greater influence at larger densities.

Our predictions for quantum wires are contrary to recent findings in quantum *wells*[8] where electron-electron scattering leads to *faster* intersubband relaxation which can be explained semiclassically [mainly by process (1122)]. However, this is consistent with our observation that the delayed relaxation is due to the *reverse* intersubband impact ionization process (2211), which is strongly enhanced by the quantum kinetic violation of energy conservation, and confirms our view that quantum kinetic effects are much more pronounced in quantum wires than in wells because of the more restricted phase space.

Our results should also be of interest for potential future applications of quantum wire structures, e.g., novel light emitting devices or a quasi-one-dimensional analog of the quantum cascade laser[52] based on intersubband population inversion, where long intersubband relaxation times are desirable. The density-dependent delay of intersubband relaxation predicted by our quantum kinetic treatment of electron-electron scattering would therefore provide a convenient means of tuning and controlling the intersubband relaxation time in quasi-one-dimensional semiconductor structures.

[1] S. H. Ashworth, M. Joschko, M. Woerner, E. Riedle, and T. Elsässer, Opt. Lett. **20**, 2120 (1996).

[2] C. Lienau, A. Richter, A. Klehr, and T. Elsässer, Appl. Phys. Lett. **69**, 2471 (1996).

[3] A. Richter, J. W. Tomm, C. Lienau, and J. Luft, Appl. Phys. Lett. **69**, 3981 (1996).

[4] M. C. Tatham, J. F. Ryan, and C. T. Foxon, Phys. Rev. Lett. **63**, 1637 (1989).

[5] N. J. Heyman, K. Unterrainer, K. Craig, B. Galdrikian, M. S. Sherwin, K. Campman, P. F. Hopkins, and A. C. Gossard, Phys. Rev. Lett. **74**, 2682 (1995).

[6] S. Lutgen, R. A. Kaindl, M. Woerner, T. Elsässer, A. Hase, H. Künzel, M. Gulia, D. Meglio, and P. Lugli, Phys. Rev. Lett. **77**, 3657 (1996).

[7] S. Lutgen, R. A. Kaindl, M. Woerner, A. Hase, and H. Künzel, Solid State Commun. **106**, 425 (1998).

[8] M. Hartig, S. Haacke, P. E. Selbmann, B. Deveaud, R. A. Taylor, and L. Rota, Phys. Rev. Lett. **80**, 1940 (1998).

[9] R. A. Kaindl, S. Lutgen, M. Woerner, T. Elsässer, B. Nottelmann, V. M. Axt, T. Kuhn, A. Hase, and H. Künzel, Phys. Rev. Lett. **80**, 3575 (1998).

[10] P. Hawrylak, J. F. Young, and P. Brockmann, Semicond. Sci. Technol. **9**, 432 (1994).

[11] K. E. Sayed, L. Bányai, and H. Haug, Phys. Rev. B **50**, 1541 (1994).

[12] E. Binder, T. Kuhn, and G. Mahler, Phys. Rev. B **50**, 18 319 (1994).

[13] M. Hartig, S. Haacke, P. E. Selbmann, B. Deveaud, R. A. Taylor, and L. Rota, Phys. Status Solidi B **204**, 159 (1997).

[14] M. Dür, S. M. Goodnick, and P. Lugli, Phys. Status Solidi B **204**, 170 (1997).

[15] V. Meden, C. Wöhler, J. Fricke, and K. Schönhammer, Phys. Rev. B **52**, 5624 (1995).

[16] L. Rota, F. Rossi, P. Lugli, and E. Molinari, Phys. Rev. B **52**, 5183 (1995).

[17] M. Herbst, V. M. Axt, T. Kuhn, and J. Schilp, Phys. Status Solidi B **204**, 358 (1997).

[18] A. Richter, G. Behme, M. Süptitz, C. Lienau, T. Elsässer, M. Ramsteiner, R. Nötzel, and K. H. Ploog, Phys. Status Solidi B **204**, 247 (1997).

[19] C. Wöhler and K. Schönhammer, Phys. Status Solidi B **204**, 362 (1997).

[20] T. D. Harris, D. Gershoni, R. D. Grober, L. Pfeiffer, K. West, and N. Chand, Appl. Phys. Lett. **68**, 988 (1996).

[21] A. Chavez-Pirson, H. Ando, H. Saito, N. Kobayashi, and H. Kanbe, Appl. Phys. Lett. **69**, 218 (1996).

[22] A. C. Maciel, C. Kiener, L. Rota, J. F. Ryan, U. Marti, D. Martin, F. Morier-Gemoud, and F. K. Reinhart, Appl. Phys. Lett. **66**, 3039 (1995).

[23] J. P. Leburton and D. Jovanovic, Semicond. Sci. Technol. **7**, B202 (1992).

[24] T. Kuhn, in *Theory of Transport Properties of Semiconductor Nanostructures*, edited by E. Schöll (Chapman and Hall, London, 1998).

[25] T. Kuhn and F. Rossi, Phys. Rev. Lett. **69**, 977 (1992).

[26] F. Rossi, S. Haas, and T. Kuhn, Phys. Rev. Lett. **72**, 152 (1994).

[27] R. Zimmermann, Festkoerperprobleme **30**, 295 (1990).

[28] R. Zimmermann, Phys. Status Solidi B **159**, 317 (1990).

[29] J. R. Kuklinski and S. Mukamel, Phys. Rev. B **44**, 11 253 (1991).

[30] R. Zimmermann, J. Lumin. **53**, 187 (1992).

[31] J. Schilp, T. Kuhn, and G. Mahler, Phys. Rev. B **50**, 5435 (1994).

[32] S. Haas, F. Rossi, and T. Kuhn, Phys. Rev. B **53**, 12 855 (1996).

[33] R. Zimmermann, J. Wauer, A. Leitenstorfer, and C. Fürst, J. Lumin. **76&77**, 34 (1998).

[34] H. Haug and S. Koch, *Quantum Theory of the Optical and Electronic Properties of Semiconductors* (World Scientific, Singapore, 1994).

[35] V. M. Axt, G. Bartels, and A. Stahl, Phys. Rev. Lett. **76**, 2543 (1996).

[36] W. Quade, E. Schöll, F. Rossi, and C. Jacoboni, Phys. Rev. B **50**, 7398 (1994).

[37] H. Schröder, H. Buss, T. Kuhn, and E. Schöll, in *Proceedings of the 9th International Conference on Hot Carriers in Semiconductors*, edited by K. Hess, J. P. Leburton, and U. Ravaioli (Plenum, New York, 1996).

[38] H. Schröder, E. Schöll, and T. Kuhn, in *Proceedings of the 23rd International Conference on the Physics of Semiconductors, Berlin 1996*, edited by M. Scheffler and R. Zimmermann (World Scientific, Singapore, 1996), Vol. 2, pp. 1157–1160.

[39] F. Prengel, E. Schöll, and T. Kuhn, Phys. Status Solidi B **204**, 322 (1997).

[40] F. Prengel and E. Schöll (unpublished).

[41] S. M. Goodnick and P. Lugli, Phys. Rev. B **37**, 2578 (1988).

[42] C. R. Bennett, M. A. Amato, N. A. Zakhleniuk, B. K. Ridley, and M. Babiker, J. Appl. Phys. **83**, 1499 (1998).

[43] J. Fricke, Ann. Phys. (N.Y.) **252**, 479 (1996).

[44] J. Fricke, V. Meden, C. Wöhler, and K. Schönhammer, Ann. Phys. (N.Y.) **253**, 177 (1997).

[45] U. Hohenester and W. Pötz, Phys. Rev. B **56**, 13 177 (1997).

[46] H. W. Wyld and B. D. Fried, Ann. Phys. (N.Y.) **23**, 374 (1963).

[47] F. Prengel, Ph.D. thesis, Technische Universität Berlin, 1998.

[48] J. Schilp, Ph.D. thesis, Universität Stuttgart, 1996.

[49] J. Schilp, T. Kuhn, and G. Mahler, Phys. Status Solidi B **188**, 417 (1995).

[50] V. Meden, J. Fricke, C. Wöhler, and K. Schönhammer, Z. Phys. B **99**, 357 (1996).

[51] K. Schönhammer and C. Wöhler, Phys. Rev. B **55**, 13 564 (1997).

[52] J. Faist, F. Capasso, C. Sirtori, D. L. Sivco, A. L. Hutchinson, M. S. Hybertsen, and A. Y. Cho, Phys. Rev. Lett. **76**, 411 (1996).